Evaluating different types of microporous materials for energy-saving atmospheric water harvest

Haonuan Zhao, Xiaobo Yang, Rémy Guillet-Nicolas, Viktar Yasnou, Valentin Valtchev

Evaluating different types of microporous materials for energy-saving atmospheric water harvest

Haonuan Zhao,[1,2] Xiaobo Yang,[2] Rémy Guillet-Nicolas,[1] Viktar Yasnou,[1] Valentin Valtchev[1,2,]*

[1] Normandie University, ENSICAEN, UNICAEN, CNRS, Laboratoire Catalyse et Spectrochimie, F-14050 Caen, France.

[2] The ZeoMat Group, Qingdao Institute of Bioenergy and Bioprocess Technology, Chinese Academy of Science, Laoshan District, CN-266101 Qingdao, China.

* Corresponding author

E-mail address: valentin.valtchev@ensicaen.fr

Abstract

Water extraction from air is a promising strategy for alleviating the current water crisis since it provides inexhaustible water resources to the places where surface and groundwater are scarce. This study systematically assesses 12 selected microporous materials out of

zeolites, aluminophosphate zeotypes (AlPOs), and metal-organic frameworks (MOFs), the most promising adsorbents to meet the stringy criteria for economic water harvesting. Through a comparative study of water adsorption isotherms, desorption enthalpies, regeneration temperatures, water capacity, and kinetics at the same condition, the zeotype aluminophosphate with AEI framework topology (AlPO-18) stands out. Using AlPO-18, 0.29 g/g water uptake is achieved in a narrow relative humidity range before 13%. The adsorbent regeneration is almost completed below 70°C. Moreover, AlPO-18 is non-toxic and the synthesis is low-cost. Therefore, AlPO-18 is a good candidate for adsorbent in developing energy-saving atmospheric water harvest (AWH) technology to extract water from "dry" air.

Keywords: Atmospheric water adsorption; Microporous materials; AlPO-18; Desorption enthalpy

1. Introduction

Freshwater scarcity is a growing global challenge. According to the United Nations Sustainable Development Goals, freshwater scarcity is the sixth most urgent issue among the current global "poly-crises".[1] It is forecasted that in 2050 more than 1/3 of urban citizens will be confronted with water scarcity.[2] Developing feasible strategies to alleviate the water crisis is urgent to avoid catastrophic changes in the living condition of a great part of the world population.

The moisture in the air may provide an alternative water resource. The water content in the Earth's atmosphere is considerable, equivalent to ~13 000 km^3, which accounts for up to

~13% of the freshwater reserve on Earth.[3] In addition, the moisture evaporated from surface water such as the ocean and the rivers spread widely through the hydrologic cycle. Atmospheric water harvest (AWH) technologies are promising to provide a sustainable water supply to places where groundwater is unavailable.

Among AWH technologies, the processes based on water adsorption/desorption cycles are practical regarding their flexibility, scalability, and easiness of implementation. However, the performances and efficiencies of such processes rely primarily on the use of efficient sorbents. Ideally, prospect materials should meet 5 criteria to enable reliable and energy-saving process developments: (1) a high water uptake capacity; (2) rapid adsorption and desorption kinetics, (3) low energy consumption for regeneration; (4) sufficient cycling stability and (5) facile and low-cost synthesis. In addition, the selected adsorbents must be non-toxic, ensuring safe implementations for both human beings and the environment.

Traditional sorption materials tested for AWH, such as silica gels, hygroscopic materials, and deliquescent liquids, failed at least one criterion.[4,5] The current research focuses on hydrophilic materials that can simultaneously fulfill all five criteria. The most promising candidates include zeolites, zeotype silicoaluminophosphates (SAPOs) and aluminophosphates (AlPOs), and metal-organic framework (MOF) materials.

Zeolites are microporous, crystalline aluminosilicates consisting of [SiO_4]-tetrahedra and [AlO_4]-tetrahedra connected by sharing vertex oxygen atoms. Their negatively charged frameworks are compensated via extra-framework metal cations.[6,7] The hydrophilicity, or hygroscopic degree, of zeolite materials is dependent on their chemical composition, i.e., the framework charges and the compensating cations. Lower framework Si/Al ratios and divalent/smaller cations generally lead to stronger hydrophilicity and larger volume for

water uptake and fast adsorption kinetics.[7,8] Most of zeolites, especially high Al containing, show type-I (IUPAC classification) water sorption isotherm and exhibit a high water capacity of ~0.2-0.45 $g_{water}/g_{zeolite}$ at 20-25°C and 0.7-1.0 P/P_0.[9–12] Typical representatives are zeolites from the LTA-type family (3A, 4A, and 5A, where the numbers refer to the effective pore size in Ångstrom) and zeolite 13X of FAU-type family that has been used as commercial desiccants. They attract attention to be considered as AWH sorbents due to their remarkable performances and cycling stability.[11,13,14] However, a disadvantage for zeolites is the high temperatures required for regeneration (> 200 °C) because water is strongly adsorbed in the micropores and interacts with compensating extra-framework cations.[8,9,14–16] High desorption temperatures may lead to a rise in energy consumption and thus reduce the cycling lifetime. In addition, zeolites usually possess poor thermal conductivity, which is also considered a weak point that results in low heat transfer efficiency. Consequently, the energy waste during the cycling processes and the heavy and bulky adsorption systems cannot be avoided.[17]

Alternatively, a new class of adsorbents, metal-organic frameworks, has been proposed. Comprising metal sites and various organic ligands, MOFs exhibit unique tunability regarding their chemical compositions and framework diversity.[18,19] These distinct properties enable the design of MOFs with desirable hydrophilicity, which makes them effective water sorbents. Recently, considerable progress has been reported in using various MOFs for water adsorption-based heat pumps, chillers, and moisture harvesting systems. However, despite the large number of developed MOFs, the long-term hydrothermal stability requirement eliminates most MOFs. UiO-66(Zr) has gained immense scientific popularity among the currently reported MOFs due to its robust structure and high stability

in aqueous, chemical, and thermal conditions. Plenty of experimental and theoretical studies evaluated water adsorption abilities in UiO-66. Measured isotherms exhibit special *S*-shape with high water capacity and speedy water uptake in the narrow range of $P/P_0 = 0.2 - 0.4$.[20,21] More importantly, UiO-66 is stable up to 450°C under air and remains intact upon water adsorption/desorption cycles by switching reversibly between dehydroxylated and hydroxylated forms[22]. This superior stability makes UiO-66 undergo a negligence decrease in cyclic water adsorption and desorption tests.[23] Coincidently, another Zr-based MOF (MOF-801) shows similar water stability.[24] Further in-depth and extensive research has acknowledged the potential and practical value of MOF-801 in enhancing the performances of adsorption-based technologies, covering from the high water uptake at drought region (down to 20% RH), the achievable solar-derived regeneration at 80°C-85°C, and the ability to improve coefficient of performance and the specific cooling power of chiller. [25–29] However, industrially available sorbents should balance performances, cost, and toxicity well. Zr-based MOFs benefit from good related properties while having some challenges on their cost and toxicity. CAU-10 is a special MOF showing advantageous stepwise water adsorption isotherm with sharp water uptake at the relative pressure $P/P_0 \approx 0.18$.[30] Fröhlich proved its excellent hydrothermal stability with as much as 700 water adsorption and desorption cycles, which reveals its good applying potential.[31] In addition, CAU-10 is formed by the connection of aluminum ions and the ligand molecules 1,3-benzene dicarboxylic acid (isophthalic acid or 1,3-H2BDC). The low price and low toxicity of aluminum salt and the isophthalic acid ligand make CAU-10 a good candidate to reach an industrial application.[32] Furthermore, water-induced decomposition/degradation of MOFs may generate organic fragments and non-

biocompatible metals,[33,34] which should also be considered since the consequent health and environmental concerns.[34–37]

Other potential candidates are the zeotype aluminophosphates. AlPOs generally show water adsorption isotherms with an *S*-shape because their neutral framework interacts less intensively with the water than zeolites.[20,21] While they usually have a water capacity similar to zeolites, the temperatures of water desorption are considerably lower (< 90 °C). For example, AQSOA-Z01, AQSOA-Z02, and AQSOA-Z05 are developed for heat pump applications. They are regenerated at 60-85°C temperature range.[22,23] Ristić et al. described the water-sorption-based energy storage performances of AlPO-18, SAPO-34, and APO-Tric at low temperatures as well.[24] The water sorption mechanism of APO-Tric was proposed to originate from a rapid and reversible change of Al coordination, causing the formation of highly ordered water clusters in a narrow pressure range. Recently, AlPO-LTA has been reported as an energy storage material with a water uptake of 0.42 g/g, and a low desorption temperature. The material is proved stable for 40 cycles.[25] Furthermore, AlPO-LTA retains its structure up to 900°C in air, proving that not all AlPOs are thermally unstable. EMM-8, another AlPO, can desorb water at 65°C, and is stable up to 700°C.[26]

All the above-discussed state-of-the-art materials, including zeolites, zeotype AlPOs, and MOFs, share a common feature; they all belong to the crystalline microporous material class. They possess strictly uniform micropores/microcages delineated by atomic frameworks that are accessible through windows of Ångstrom dimension. The present paper provides a comprehensive evaluation of these sorbents regarding their performances as moisture harvesters. Zeolite A, zeolite 13X, SAPO-34, AlPO-18, AlPO-34, EMM-8, as well as CAU-10, MOF-801, and UiO-66 have been chosen as representatives of the 3 main

material classes. They have all been reported previously to have outstanding properties in one or another aspect of water capacity, regeneration, and recyclability. In the present study, the critical parameters, such as adsorption isotherms, desorption temperatures, and cycling stabilities, are carefully determined using the same measurement conditions to allow direct comparisons. Assessing the results against the 5 criteria, we emphasize that AlPO-18 stands out. A detailed analysis of the results and the investigated parameters reveals the superiority of AlPO-18 when all 5 parameters are taken into account.

2. Experimental

2.1. Synthesis of microporous sorbents

2.1.1. Chemicals and Materials

All chemicals were used as purchased: sodium aluminate ($NaAlO_2$, 50 % Al_2O_3 and 45 % Na_2O, Sigma-Aldrich), sodium silicate (Na_2SiO_3, reagent grade, Sigma-Aldrich), sodium hydroxide (NaOH, 98%, Thermoscientific), tetraethyl orthosilicate (TEOS, > 99.0%, Sigma-Aldrich), Aluminum isopropoxide (> 98%, Thermoscientific), aluminum sulfate octadecahydrate ($Al_2(SO_4)_3 \cdot 18H_2O$, 99%, Rectpur), zirconyl chloride octahydrate ($ZrOCl_2 \cdot 8H_2O$, > 99.5%, Sigma-Aldrich), lithium nitrate ($LiNO_3$, 99%, Thermoscientific), calcium nitrate ($Ca(NO_3)_2 \cdot 4H_2O$, 99%, R. P. Normapur. AR), magnesium nitrate ($Mg(NO_3)_2$, 99%, Sigma-Aldrich), orthophosphoric acid (H_3PO_4, 85 wt.% aq., Alfa Aesar), hydrochloric acid (HCl, 37 wt.% aq., Fisher Chemical), hydrofluoric acid (HF, 40 wt.% aq., Macklin), tetraethylammonium hydroxide (TEAOH, 35 wt.% aq., Alfa Aesar), piperidine (analysis pure, Merk), 4-dimethylaminopyridine (4-DMAP, > 99%, Tokyo Chemical Industry co., LTD), 1,3-benzenedicarboxylic acid (1,3-H_2BDC, 99%, Sigma-Aldrich), *N*,*N*-dimethylformamid (DMF, > 99%, Thermoscientific), terephthalic acid (98%, Sigma-

Aldrich), fumaric acid (99%, Thermoscientific), formic acid (99%, Carlo erba reagents), commercial zeolite 13X (Merck), commercial SAPO-34 (Alfa Chemistry). Deionized (DI) water was used in the synthetic experiments.

2.1.2. Synthesis

Table 1 The synthetic recipes, hydrothermal parameters, and corresponding products.

EXP #	Gel composition	Temperature (°C)	Time	Material
1	3.615 Na_2O: 1.0 Al_2O_3: 1.926 SiO_2: 128 H_2O	100°C	4 hours	NaA
2	1.0 Al_2O_3: 2.0 P_2O_5: 0.6SiO_2: 4.0 TEAOH: 75 H_2O	150°C	1 day	SAPO-34
3	0.8Al_2O_3: 2.0 P_2O_5: 4.0 TEAOH: 75 H_2O	150°C	3 days	AlPO-18
4	0.5 Al_2O_3: 1.0 P_2O_5: 2.0 piperidine: 1.0 HF: 100 H_2O	200°C	4 days	AlPO-34
5	0.5 Al_2O_3: 1.0 P_2O_5: 2.0 4-DMAP: 40 H_2O	180°C	3 days	EMM-8
6	1 1,3-H_2BDC: 1 $Al_2(SO_4)_3 \cdot 18H_2O$: 10.77 DMF: 185.18 H_2O	135 °C	13 hours	CAU-10
7	1 $ZrOCl_2 \cdot 8H_2O$: 1 fumaric acid: 51.66 DMF: 37.11 formic acid	150°C	50 hours	MOF-801
8	1.35 terephthalic acid: 1 $ZrOCl_2 \cdot 8H_2O$: 358.76 DMF: 59.94 HCl	150°C	15 hours	UiO-66

Table 1 summarizes the synthetic recipes. Further experimental details are described in Supporting Information section S1. Benchmark zeolites and zeotype materials, including NaA[27], SAPO-34[27], AlPO-34[28], AlPO-18[29], and EMM-8[26] were hydrothermally synthesized. CAU-10[30], MOF-801[31], and UiO-66[32] were prepared by solvothermal synthesis using the reported recipes.

To get different cationic forms of zeolite LTA, Na-form zeolite A was used as the parent material and ion-exchanged. Mg^{2+}, Ca^{2+} and Li^{+}-exchanged zeolite A were prepared: 3 grams of calcined NaA were dispersed in 120 ml 0.5 mol/L corresponding metal nitrate solution and stirred at 80°C for 3 hours for 3 times.

Before the adsorption analyses, zeolites and zeotypes were calcined in air at 550°C for 5 hours. MOFs were activated at 150°C overnight.

2.2. Characterization

Crystalline products were identified by powder X-ray diffraction at room temperature in ambient air on an Anton Paar XRDynamic 500 diffractometer using Cu-Kα radiation (k = 1.5418 Å, 40 kV, 50 mA). The analysis was conducted at a scanning rate of 0.03 °/min in the region of 2θ = 5°- 40°. Structural stability of AlPO-18 was characterized by temperature-programmed X-ray in XRK 900 thermocouple sample holder in steps of 100°C up to 900°C.

Scanning Electron Microscopy (SEM) on Tescan Mira I LMH under 30 kV was used to study samples' morphology. Inductively coupled plasma mass spectrometry (ICP-MS) was performed on a 7900 ICP-MS from Agilent Technologies for the elemental analysis.

Nitrogen adsorption and desorption isotherms were obtained at 77 K on Micromeritics 3Flex Surface Characterization unit (Norcross, GA). Prior to the test, samples were outgassed at 200°C in vacuum for 4 hours. To characterize the pore information, BET (Brunauer-Emmett-Teller) model was used to determine samples' surface area, and t-plot method associated with Broekhoff-de Boer equation was used for checking micropore volume.

The thermal desorption analyses were completed with the assistance of a thermogravimetric analyzer (NETZSCH STA 449F3) connected to a differential scanning calorimeter. Experiments were carried out in the nitrogen flow of 40 ml/min and at the heating rate of 1°C/min till 200°C for AlPOs and MOFs or 500°C for zeolites and SAPOs. The same conditions are used for the measurement of desorption enthalpies. All samples

were exposed to controlled relative humidity (RH) of 75% for over 3 days to ensure saturation with water vapor prior to the analyses.

The water capacities of sorbents are calculated with equation (1):

$$\text{Water capacity}\left(\frac{g_{H_2O}}{g_{Sorbent}}\right) = \frac{\text{Water loss(g)}}{\text{Initial weight(g)-Water loss(g)}} \#(1)$$

Water losses here are obtained from thermogravimetric analyses.

The energy consumptions during regeneration were measured through the calorimetric method. Water desorption happened together with special endothermal peaks in the DSC curve. By integrating the peak over time and DSC signal (in the unit of W/g), the integral areas were recorded, which are regarded as the energy consumption in the unit of J/g. For easy comparison with other studies, the energy consumptions in $kWh/g_{sorbents}$ were calculated by multiplying the values in units of J/g with 2.78×10^{-7}. Also, desorption enthalpies with the unit of kJ/mol_{water} were calculated through equation (2):

$$\text{Desorption enthalpy}\left(\frac{\text{kJ}}{\text{mol}_{water}}\right) = \frac{\text{Energy consumption(kJ/g)}}{\text{Water capacity(g/g)/18 (g/mol)}} \#(2)$$

2.3. Water adsorption measurements

The isotherms of water adsorption and desorption were measured with a dynamic vapor sorption analyzer (DVS vacuum, Surface Measure Systems P20F0046) in RH between 0-90% and at 25°C.

The water adsorption cycling test for AlPO-18 was carried out with the following sequential procedure: AlPO-18 was dehydrated at 150°C under vacuum until a constant weight was achieved. Then, dry AlPO-18 powder was hydrated at 75% RH until saturated, followed by dehydrating at 150°C under a high vacuum to a constant mass.

Water adsorption kinetic measurements were performed on DVS in 30% RH at 25 °C. All samples were shaped in size between 0.4 mm - 0.5 mm to mitigate the dimension effect. After *in situ* activation at an elevated temperature (350°C for zeolites, 200°C for SAPO/AlPOs, and 150°C for MOFs) for several hours, all samples were exposed to humidity immediately and kept for 2 hours.

3. Results and discussion

3.1. The materials

The water adsorption capacity, desorption temperatures, and cyclability are the three main criteria for evaluating microporous materials selected for the study. All these parameters are required characteristics for efficient AWH. The set of materials involved in the study is (1) zeolites - self-prepared and ion-exchanged zeolite A, commercial zeolite 13 X; (2) zeotypes - AlPOs and SAPOs, i.e., AlPO-18, AlPO-34, EMM-8, SAPO-34 (all self-prepared), and a commercial SAPO-34; (3) MOFs - including CAU-10, MOF-801 and UiO-66 (all synthesized). The framework structures and relevant micropore/cage features are shown in Figure S1-S2 and Table S1 which are described in section S2 of the Supporting Information.

The powder XRD patterns in Figure S3-S10 in the Supporting Information prove that the synthesized zeolite NaA, zeotype AlPO-18, AlPO-34, SAPO-34, and EMM-8, as well as the MOFs CAU-10, MOF-801, and UiO-66 are phase-pure and highly crystalline.

For AlPO materials (Figure S5-S7), XRD patterns reveal that their structures undergo certain changes upon calcination. AlPO-18 and AlPO-34 still exhibit sharp diffraction peaks, but new peaks appear in addition to the changes in relative intensities of existing

ones. This is due to the low symmetry transformation upon SDA removal and hydration.[33–35] SAPO-34 and EMM-8 show more significant peak broadening after calcination. The water-induced and calcination-caused structure change could be responsible for this phenomenon.

However, according to previously reported studies, the framework connectivity is retained in all cases.[28,34]

Zeolites LiNaA, CaNaA, and MgNaA were prepared by 3 consecutive ion-exchange cycles using NaA zeolite. The results of elemental analysis and the extent of the ion-exchange are given in Table 2. The parent NaA consists of strictly alternating silicon and aluminum atoms leading to a Si/Al ratio close to 1, which is the minimum value allowed by Loewenstein's rule, thus the highest cation content for all zeolites.[36]

Crystalline MOFs were successfully synthesized according to the literature[30–32]. XRD (Figure S8-S10) confirms that they are highly pure and highly crystalline.

Table 2 Chemical composition of different ion-exchanged forms of LTA-type zeolites determined by ICP.

Samples	Molar ratio			
	Na/Al	Cation/Al	(Na + n M^{n+})/Al	Ion-exchange degree
NaA	0.91	0	0.91	100%
LiNaA	0.21	0.79	1.00	77%
CaNaA	0.04	0.42	0.88	96%
MgNaA	0.12	0.38	0.88	87%

3.2. Evaluation of water adsorption properties

3.2.1. Water adsorption isotherms

Figure 1 shows the water adsorption isotherms measured at 25°C for zeolites, zeotypes, and MOFs. The zeolites present typical type I curves (Figure 1a), which indicate their strong affinity to water molecules under low humidity. Indeed, the isotherms are characterized by remarkable uptakes in the low-pressure region. In addition to the energetically favored micropore-filling process, the extra-framework cations play a significant role in water adsorption. For the monovalent ions, Li^+ has a smaller size as compared to Na^+ (0.69 Å *vs* 1.02 Å in radius, respectively), and thus has a stronger electrostatic affinity to water. Therefore, LiNaA's isotherm exhibits a larger uptake at low pressures. The divalent ion Ca^{2+} has an even higher charge density, but its size is also bigger (1.0 Å), canceling the gains in the electrostatic affinity. CaNaA isotherm falls at the same level as NaA and LiNaA. MgNaA stands out regarding water uptake because Mg^{2+} ion benefits from higher charges and smaller radius (0.72 Å).[37,38] For comparison, the isotherm of a commercial 13X zeolite (NaX, Si/Al~1.2) has the same shape but slightly higher capacity than NaA and LiNaA, which originates from its bigger channel opening and more available cavity.

The zeotype AlPOs have significantly different behavior from zeolites because of their different framework compositions, although they still have zeolitic microporous structures. Compared with the zeolites, the leap of SAPO-34's isotherm shifts towards a higher P/P_0 at ~0.1 due to the decreasing strength of the water-framework interaction. AlPO-18, AlPO-34, and EMM-8 illustrate the typical sigmoid isotherms with stepwise water adsorption consisting of limited adsorption in the low pressures followed by a sharp increase in a

narrow pressure range around P/P_0 = 0.10-0.13, 0.06-0.11, and 0.11-0.20, respectively. This unusual adsorption behavior mainly originates from the sudden micropore filling of water molecules induced by hydrogen bonding and the reversible coordination change of framework aluminum.[26,39,40] This particular water adsorption behavior is advantageous because the desorption would consume less energy.[24] Moreover, AlPO-18 exhibits a water uptake of 0.30 g/g at P/P_0 = 0.2, which is higher than most of the small pore zeolites and zeotype materials under the same condition, MgNaA excepted (0.31 g/g at P/P_0 = 0.2).

When P/P_0 arises close to the vapor saturation pressure, MOF-801 has the highest water capacity, reaching around 0.43 g/g at P/P_0 = 0.9. All MOFs show *S*-shaped isotherms. But the main adsorption processes in UiO-66 and MOF-801 stretch over broader pressure ranges as compared to AlPOs, revealing a slower and more progressive adsorption process. Main uptake of the isotherm is got at P/P_0 = 0.06-0.15 for MOF-801, 0.15-0.18 for CAU-10, and 0.20-0.4 for UiO-66.

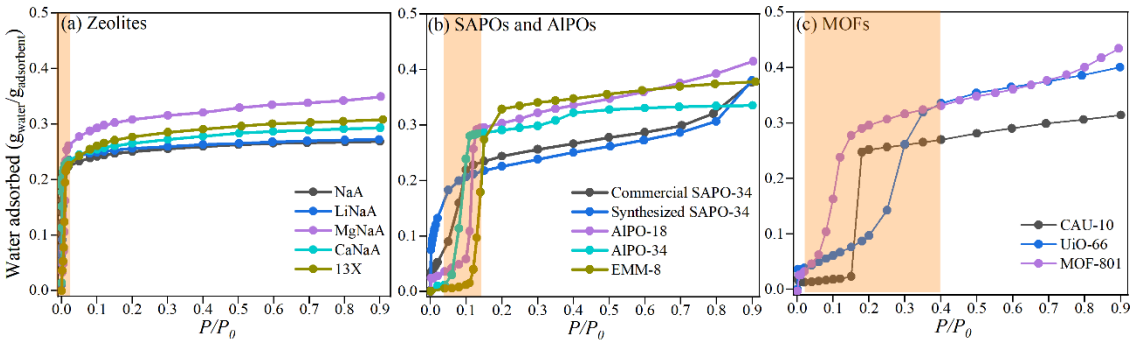

Fig. 1. Water adsorption isotherms at 25°C of zeolites (a), SAPOs and AlPOs (b), and MOFs (c).

3.2.2. Regeneration and energy consumption

The water saturation capacity and the desorption enthalpy were determined by means of thermogravimetric and calorimetric measurements. The samples were calcined and hydrated under 75% RH at room temperature before the test. Figure 2 and Table 3 illustrate the water capacity (desorbed amount), desorption temperature, and energy consumption that were needed to dry the samples. The desorption of water from hydrated zeolites occurs in a broad temperature range, starting below 100°C and finishing above 300°C (Figure S11). The energy consumption to regenerate a gram of zeolite A is 0.81-1.03 Wh, the highest value among the 3 tested materials. The corresponding energy costs for water production are 173 to 230 kJ per mol water, with MgNaA being the most energy-intensive example. These values could be significantly reduced by changing the framework chemical composition. SAPO-34 is generally classified as mildly acidic, and its acidity could be varied by modifying the synthesis conditions.[41] Originating from the lower acidity, SAPO-34 exhibits moderate hydrophobicity. It is more hydrophobic than zeolite materials which has been proved by the isotherms. The water desorption process for SAPO-34 finishes at around 200°C with a peak located at 54-64°C. The energy consumed to regenerate SAPO-34 is almost half of that for zeolite samples; only around 0.47 Wh/g was the cost for drying the commercial SAPO-34. This trend becomes more obvious in aluminophosphate samples with neutral frameworks. AlPOs dehydrate at below 100°C, which is much lower than that of zeolites and SAPO-34, and is very advantageous for the considered application. For AlPO-18, AlPO-34, and EMM-8 samples, complete dehydration can be achieved between 57°C and 94°C, corresponding to 0.27-0.38 Wh/g energy consumption. These energy consumptions are only 30%-50% of the ones of zeolite material. Noteworthy, AlPO-18 almost completes its regeneration at ~70°C (Figure S12),

and exhibits the lowest heat consumption (0.27 Wh/g) among all AlPOs. The regeneration energy is comparable to the MOF-801 (0.27 Wh/g). In other words, ~50 kJ energy is needed to release a mole of water trapped in the AlPO-18's structure, which is close to the evaporation enthalpy of liquid water at 25°C (-44 kJ/mol). Compared to most of the currently reported zeolites or SAPOs, AlPOs are claimed to be outstanding at energy-saving regenerations and allow high uptake of water at slightly higher pressures. Therefore, they can efficiently extract water from "dry" air, and be energy-savingly regenerated.

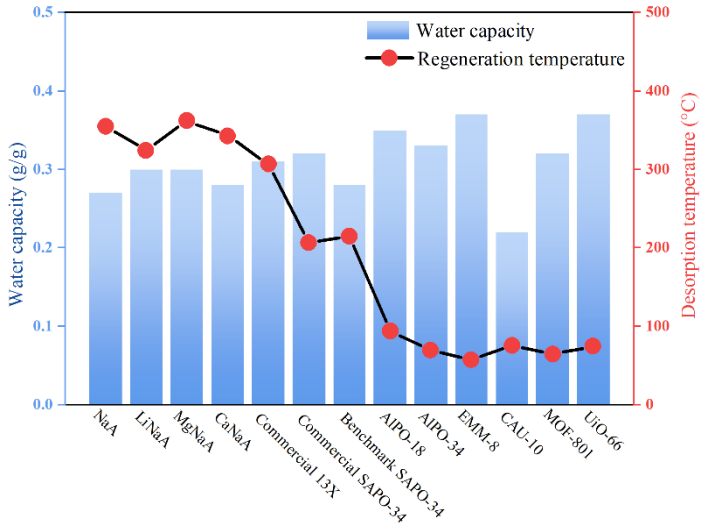

Fig. 2. Water capacity as desorption amount measured in TG analysis (hydrated under 75% RH at 25 °C) and temperatures for complete desorption.

On the other hand, MOFs provide low water desorption temperatures as well. Complete water desorption from MOFs happens at 64-80°C, with a maximum peak at 40-53°C temperature range. This is similar to the behavior observed for AlPOs. UiO-66 is the most effective among the selected MOFs, with the highest water capacity (0.36 g/g) and lowest desorption temperature (80°C with a maximum at 40°C). An energy cost of 0.27 Wh/g was

observed for MOF-801, which is 70% and 28% higher than that of CAU-10 and UiO-66. These properties make MOF materials also promising water sorbents, but the water-induced MOF degradation and the difficulty in their scalable production must be considered before their real application.

Table 3 TG/DSC and calorimetric data. Samples were hydrated under 75% RH at 25°C.

Samples	Desorption meak maximum (°C)	Energy consumption ($Wh/g_{sorbents}$)	Desorption enthalpy (kJ/mol_{water})
NaA	101	0.94	225
LiNaA	96	0.81	173
MgNaA	82, 114	1.03	220
CaNaA	143	1.00	230
Commercial 13X	111	0.96	200
Commercial SAPO-34	54	0.47	94
Benchmark SAPO-34	64	0.61	140
AlPO-18	61	0.27	50
AlPO-34	65	0.38	75
EMM-8	52	0.29	50
CAU-10	53	0.16	42
MOF-801	49	0.27	53
UiO-66	40	0.21	37

3.2.3. Water adsorption kinetics

Figure 3 plots the water uptake profiles as a function of time. Uniform grains of 0.4-0.5 mm were used in the tests. Zeolites start to adsorb water immediately when exposed to moisture. The shape of the curves shows a fast increase in the first 30-60 min, followed by a quick equilibrium. This shape is similar to the previous reports in zeolite LTA, CHA and 13X.[42,43] Water adsorption kinetic is related to the slope of the curve profile, while the slopes in each curve are slightly different depending on the species of framework compensation cations. Water molecule binds strongly with smaller cations because of the dipole moment, providing shorter distances for interaction with the center of the adsorbate. The water equilibrium on LiNaA is reached 20 min earlier than on NaA. The water adsorption rates decrease according to the order LiNaA ≈ CaNaA > MgNaA > NaA. Benefiting from the large channel, 13X adsorbs water faster than NaA, but at a similar speed to MgNaA.

The water adsorption in zeotypes shows a two-step profile. As to SAPO-34, water is adsorbed slowly from time zero due to its weaker interaction with the framework than zeolites. Then a rapidly saturation is achieved during the 45^{th} to 65^{th} min. The sudden change of adsorption kinetics at the 40^{th} minute is attributed to the change in aluminum coordination[44]. AlPO-18 exhibits a similar two-step profile, with rapid saturation in the 40^{th} to 50^{th} minute, and 80% (0.24 g/g) water uptake is achieved in the second step. AlPO-18 does not have strong acid sites, but the pore structure changes with water coverage, which requires further in-depth studies to be fully understood. AlPO-34 and EMM-8 show a profile with delayed and sharp water uptakes, being saturated in a single step within approximately 10 min starting at the 45^{th} and 50^{th} minute, respectively. The consistency in

the water adsorption behavior of AlPOs inevitably brings to mind the structural alterations occurring with water coverage in AlPOs. Much like the discussion above for the isotherms, the migration of water molecules and their proximity to the framework aluminum atoms induce a change in the coordination number of Al atoms,[44,55,56] consequently leading to structure distortion. The water-induced structural change and the structure-induced water adsorption behavior modifications have been reported in a few cases. However, this topic remains largely understudied, and hence future studies are highly recommended. Even so, the probably triggered pronounced surge in adsorption kinetics give important information for practical usage of zeotype materials.

Coincidentally, the water adsorption profiles of MOFs show a similar curve shape as AlPO-18. Zr-based MOF-801 and UiO-66 show higher hydrophilicity than Al-based CAU-10. MOF-801 harvests ~0.18 g/g water at the second stage, from 50^{th} to 60^{th} min, which is 67% of its total uptake. The dominating sorption step in UiO-66 starts after its exposure to humidity for 50 min, showing a certain delay with respect to other MOFs. The adsorption grows in the following 1 hour, and does not reach the saturation. The slow kinetic is an obvious disadvantage of UiO-66.

Above all, all the sorbents show obvious *S*-shaped water loading curves except zeolites, containing a speedy water adsorption process. The sharp increase of adsorption kinetics-related slope in zeotypes and MOFs implies the potential working condition for these materials. The faster water uptake kinetics in their suitable working range could allow more water harvest-release cycles in a given time, thereby yielding more water from a space-saving setup.[45]

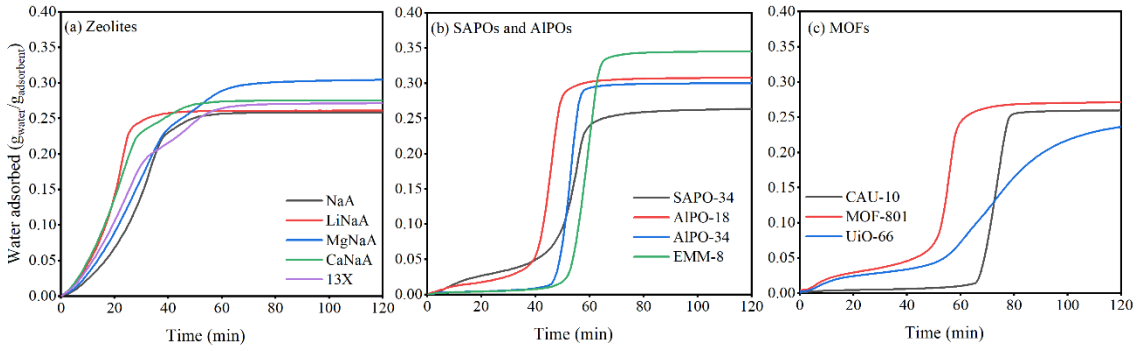

Fig. 3. Water adsorption profiles of zeolites (a), SAPOs and AlPOs (b), and MOFs (c) at 25°C in relative humidity at 30%. The material grains are 0.4-0.5 mm.

3.3. AlPO-18 as water adsorbent

The detailed comparative studies highlighted that the zeotypes AlPO-18, AlPO-34 and EMM-8 are very effective in realizing affordable, energy-saving and high-performance water adsorption. In recent years AlPO-34 and EMM-8 have been thoroughly inspected as alternatives for low-temperature-driven water sorption-based air-conditioning, with performances competing with MOFs.[24,26] So far, AlPO-18 has been less studied, but it is another effective material that has been found to be equally advantageous as AlPO-34 and EMM-8.

The framework structure of AlPO-18 (AEI) can be described as a stack of double 6 rings and is a distortion of chabazite structure (Figure 4a). It shows 3-dimensional 8-ring channels with a slightly elliptical cross-section (Supporting Information Section 2). Scanning electron microscopy inspection shows the two-edged sword-shaped crystals of AlPO-18 (Figure 4b). The thickness of the plates is distributed around 20~50 nm.

The nitrogen adsorption isotherm (Figure 4c) reveals that AlPO-18 has a high BET surface area of 656 m^2/g, and a pore volume of 0.31 cm^3/g. According to the t-plot method,

the micropore volume of AlPO-18 is 0.22 cm^3/g. The large external surface area is an expected consequence of the ultra-thin morphology and agrees well with the data reported previously[46,47]. The *in situ* XRD patterns of as-synthesized AlPO-18 were collected at elevated temperatures in the air. With respect to the TGA (Figure S13), the degradation and combustion of the organic structure-directing agent (SDA: TEA^+ in this case) begin at around 350°C. After the SDA removal, the material retains a high crystallinity. But the shifts and recombination of some reflection peaks indicate a change in the lattice symmetry. The as-synthesized AlPO-18 can be described in the orthorhombic symmetry *Cmcm*. After calcination, the framework has tilted to the monoclinic symmetry *C*2/*c*.[35,39]

AlPO-18 exhibits remarkable thermal stability up to at least 900 °C. The intensity of diffraction peaks doesn't show significant reduction, and the XRD peaks remain sharp. This thermal stability reveals the robust structure of AlPO-18, which is also reported in AlPO-34 and AlPO-LTA,[25] while slightly higher than that of EMM-8.[26]

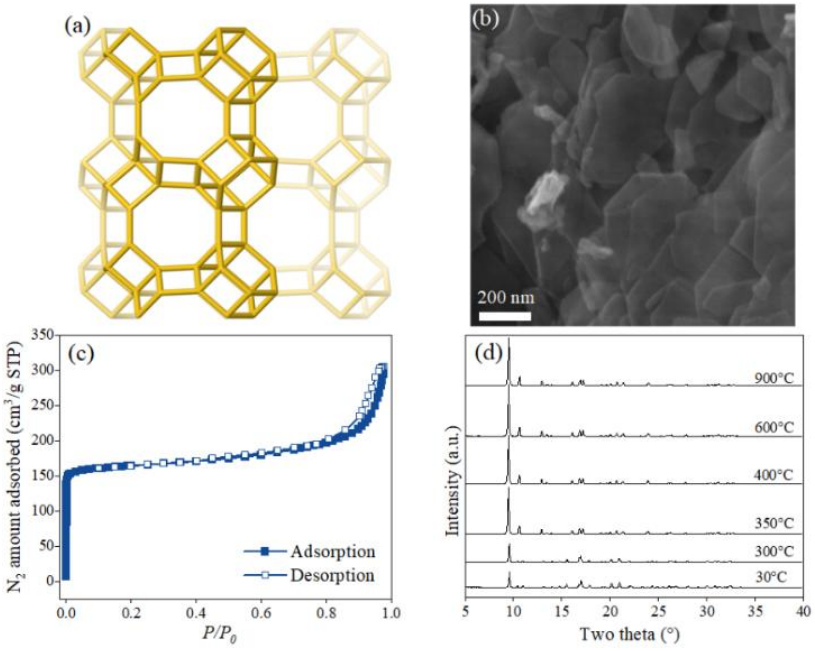

Fig. 4. The framework structure of AlPO-18 (a), SEM micrograph of AlPO-18 (b), Nitrogen adsorption/desorption isotherm (c), and temperature-dependent *in situ* powder X-ray diffraction of (as-synthesized) AlPO-18 (d).

Figure 5a illustrates the water adsorption/desorption isotherm on AlPO-18 at 25°C. A sharp water uptake occurs in the narrow range of P/P_0 = 0.10-0.13. And there is a hysteresis between the desorption/adsorption branches. The dynamic water sorption experiment shown in Figure 5b illustrates the process in detail: 0.30 g/g water is adsorbed at a low relative humidity of 13%, which accounts for ~ 70% of its total water capacity (0.42 g/g). This main adsorption step reaches equilibrium relatively fast, demonstrating favorable kinetics in the narrow RH range between 10% to 13%, while the sharp desorption of a similar amount (0.23 g/g) happens between 8% and 4% RH. The existence of the narrow hysteresis loop is a common phenomenon for water adsorption on AlPO materials. It is repeatable in the following several rounds and doesn't change its position or range (Figure S14). Also, it can be advantageous since it enables water holding and delivery with the constant RH gap between adsorption and desorption. Water adsorption/desorption cycling stability is another key factor that plays a crucial role in water yield and sorbent lifetime. To accelerate water desorption and examine the hydrothermal stability of AlPO-18, a harsh condition has been set for regeneration in the cyclic test. Figure 5c demonstrates the multi-cyclic test of water adsorption and desorption on AlPO-18. Water vapor was adsorbed at 25°C while regenerated after each cycle at 150°C. Figure 5c demonstrates the multi-cyclic test of water adsorption and desorption on AlPO-18. Water vapor was adsorbed at 25°C while regenerated after each cycle at 150°C. Over 10 cycles, the uptake capacity decreases

slightly, by ca. 0.01 g/g, probably because the low crystalline parts of AlPO-18 are amorphized upon steaming (Figure 5d). In addition, the first adsorption takes a longer time before the steep uptake. That originates from the fact that the first adsorption round accounts not only for the water uptake but also reflects the chemical nature of the sorbent and its surface-wetting behavior upon increasing humidity.

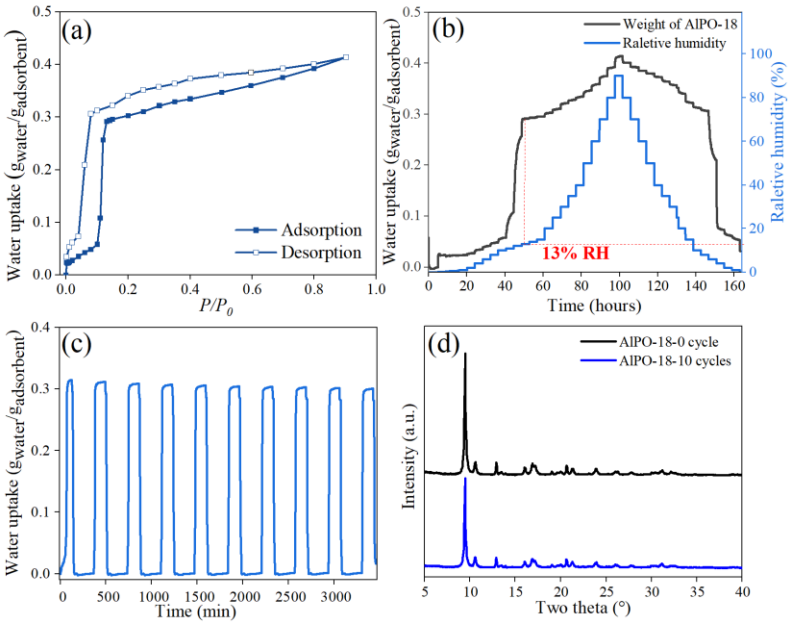

Fig. 5. Water adsorption and desorption isotherm of AlPO-18 at 25°C (a), dynamic water adsorption profile in AlPO-18 (b), hydration and dehydration cycling performance of AlPO-18 (c), XRD spectra of fresh dehydrated AlPO-18 and the same sample after 10 cycles of water adsorption and desorption.

4. Conclusions

Crystalline microporous materials of the classes zeolites, AlPO zeotypes, and metal-organic frameworks (MOFs), reported on various occasions for their potential for atmospheric water harvest (AWH) applications, have been systematically studied. Zeolite

13X, different cationic forms of zeolite A, the zeotype AlPO-18, AlPO-34, SAPO-34, and EMM-8, as well as CAU-10, MOF-801, and UiO-66 have been chosen as representatives of respective classes, and assessed for their water adsorption isotherms, desorption temperatures, energy consumption, as well as cycling performances.

Zeolites have been proven to extract water deeply from dry air with very low humidity, but the regeneration is energy-intensive. The set of experimental data confirmed that MOFs are advantageous in energy-saving regenerations at low temperatures and high water-uptake capabilities. However, their adsorption is extended in a relatively large temperature range. AlPO materials stand out by combining high water capacity in a narrow and operational humidity range, and facile desorption at low temperatures comparable to MOFs.

The small-pore AlPO-18 has been thoroughly studied. It is suitable to extract water in a narrow range of relative humidity (10%-13%), and being almost completely regenerated below 70°C. These conditional parameters are favored for facile designs of energy-saving cycling processes. Moreover, AlPO-18 is thermally stable for at least 900°C. Therefore, AlPO-18 is a potential candidate for sorption-based AWH technology.

CRediT authorship contribution statement

Haonuan Zhao: Writing – original draft, Data curation, Investigation, Formal analysis. **Xiaobo Yang:** Investigation, Methodology, Validation, Writing – review & editing. **Rémy Guillet-Nicolas:** Writing – review & editing, Validation, Formal analysis. **Viktar Yasnou:** Project administration, Validation, Formal analysis. **Valentin Valtchev:** Supervision, Project administration, Funding acquisition, Conceptualization, Writing – review & editing.

Declaration of competing interest

There are no conflicts to declare.

Acknowledgments

Valentin Valtchev and Viktar Yasnou acknowledge the support in the pre-maturation project ZEAU (CNRS) framework. Haonuan Zhao and Valentin Valtchev acknowledge the support of China Scholarship Council. Rémy Guillet-Nicolas and Valentin Valtchev acknowledge the support of the Region Normandy through the Chair of Excellence. This work has been carried out within the Sino-French International Research Network "Zeolites" frame.

References

[1] The water crisis is worsening. Researchers must tackle it together, Nature 613 (2023) 611–612. https://doi.org/10.1038/d41586-023-00182-2.
[2] W. Shi, W. Guan, C. Lei, G. Yu, Sorbents for Atmospheric Water Harvesting: From Design Principles to Applications, Angew. Chem. 134 (2022) e202211267. https://doi.org/10.1002/ange.202211267.
[3] F. Zhao, X. Zhou, Y. Liu, Y. Shi, Y. Dai, G. Yu, Super Moisture-Absorbent Gels for All-Weather Atmospheric Water Harvesting, Adv. Mater. 31 (2019) 1806446. https://doi.org/10.1002/adma.201806446.
[4] X. Zhou, H. Lu, F. Zhao, G. Yu, Atmospheric Water Harvesting: A Review of Material and Structural Designs, ACS Mater. Lett. 2 (2020) 671–684. https://doi.org/10.1021/acsmaterialslett.0c00130.
[5] J. Xu, T. Li, J. Chao, S. Wu, T. Yan, W. Li, B. Cao, R. Wang, Efficient Solar-Driven Water Harvesting from Arid Air with Metal–Organic Frameworks Modified by Hygroscopic Salt, Angew. Chem. Int. Ed. 59 (2020) 5202–5210. https://doi.org/10.1002/anie.201915170.
[6] A. Palčić, V. Valtchev, Analysis and control of acid sites in zeolites, Appl. Catal. Gen. 606 (2020) 117795. https://doi.org/10.1016/j.apcata.2020.117795.

[7] C. Wang, H. Guo, S. Leng, J. Yu, K. Feng, L. Cao, J. Huang, Regulation of hydrophilicity/hydrophobicity of aluminosilicate zeolites: a review, Crit. Rev. Solid State Mater. Sci. 46 (2021) 330–348. https://doi.org/10.1080/10408436.2020.1819198.
[8] V.R. Mollo-Varillas, F. Bougie, M.C. Iliuta, Selective adsorption of water vapor in the presence of carbon dioxide on hydrophilic zeolites at high temperatures, Sep. Purif. Technol. 282 (2022) 120008. https://doi.org/10.1016/j.seppur.2021.120008.
[9] E.-P. Ng, S. Mintova, Nanoporous materials with enhanced hydrophilicity and high water sorption capacity, Microporous Mesoporous Mater. 114 (2008) 1–26. https://doi.org/10.1016/j.micromeso.2007.12.022.
[10] M. Tatlier, G. Munz, S.K. Henninger, Relation of water adsorption capacities of zeolites with their structural properties, Microporous Mesoporous Mater. 264 (2018) 70–75. https://doi.org/10.1016/j.micromeso.2017.12.031.
[11] K.-M. Kim, H.-T. Oh, S.-J. Lim, K. Ho, Y. Park, C.-H. Lee, Adsorption Equilibria of Water Vapor on Zeolite 3A, Zeolite 13X, and Dealuminated Y Zeolite, J. Chem. Eng. Data 61 (2016) 1547–1554. https://doi.org/10.1021/acs.jced.5b00927.
[12] A.A. Dabbawala, K. Suresh kumar Reddy, H. Mittal, Y. Al Wahedi, B.V. Vaithilingam, G.N. Karanikolos, G. Singaravel, S. Morin, M. Berthod, S.M. Alhassan, Water vapor adsorption on metal-exchanged hierarchical porous zeolite-Y, Microporous Mesoporous Mater. 326 (2021) 111380. https://doi.org/10.1016/j.micromeso.2021.111380.
[13] E. Jaramillo, M. Chandross, Adsorption of Small Molecules in LTA Zeolites. 1. NH_3, CO_2, and H_2O in Zeolite 4A, J. Phys. Chem. B 108 (2004) 20155–20159. https://doi.org/10.1021/jp048078f.
[14] G. Santori, A. Frazzica, A. Freni, M. Galieni, L. Bonaccorsi, F. Polonara, G. Restuccia, Optimization and testing on an adsorption dishwasher, Energy 50 (2013) 170–176. https://doi.org/10.1016/j.energy.2012.11.031.
[15] Y. Yuan, H. Zhang, F. Yang, N. Zhang, X. Cao, Inorganic composite sorbents for water vapor sorption: A research progress, Renew. Sustain. Energy Rev. 54 (2016) 761–776. https://doi.org/10.1016/j.rser.2015.10.069.
[16] G. Martra, R. Ocule, L. Marchese, G. Centi, S. Coluccia, Alkali and alkaline-earth exchanged faujasites: strength of Lewis base and acid centres and cation site occupancy in Na- and BaY and Na- and BaX zeolites, Catal. Today 73 (2002) 83–93. https://doi.org/10.1016/S0920-5861(01)00521-1.
[17] M.B. Jakubinek, B.-Z. Zhan, M.A. White, Temperature-dependent thermal conductivity of powdered zeolite NaX, Microporous Mesoporous Mater. 103 (2007) 108–112. https://doi.org/10.1016/j.micromeso.2007.01.040.
[18] H.-C. Zhou, J.R. Long, O.M. Yaghi, Introduction to Metal–Organic Frameworks, Chem. Rev. 112 (2012) 673–674. https://doi.org/10.1021/cr300014x.
[19] H. Furukawa, K.E. Cordova, M. O'Keeffe, O.M. Yaghi, The Chemistry and Applications of Metal-Organic Frameworks, Science 341 (2013) 1230444. https://doi.org/10.1126/science.1230444.
[20] T. Kohler, M. Hinze, K. Müller, W. Schwieger, Temperature independent description of water adsorption on zeotypes showing a type V adsorption isotherm, Energy 135 (2017) 227–236. https://doi.org/10.1016/j.energy.2017.06.115.

[21] K.C. Ng, M. Burhan, M.W. Shahzad, A.B. Ismail, A Universal Isotherm Model to Capture Adsorption Uptake and Energy Distribution of Porous Heterogeneous Surface, Sci. Rep. 7 (2017) 10634. https://doi.org/10.1038/s41598-017-11156-6.
[22] H. Wei Benjamin Teo, A. Chakraborty, W. Fan, Improved adsorption characteristics data for AQSOA types zeolites and water systems under static and dynamic conditions, Microporous Mesoporous Mater. 242 (2017) 109–117. https://doi.org/10.1016/j.micromeso.2017.01.015.
[23] K.A. Rocky, A. Pal, T.H. Rupam, Nasruddin, B.B. Saha, Zeolite-graphene composite adsorbents for next generation adsorption heat pumps, Microporous Mesoporous Mater. 313 (2021) 110839. https://doi.org/10.1016/j.micromeso.2020.110839.
[24] A. Ristić, N.Z. Logar, S.K. Henninger, V. Kaučič, The Performance of Small-Pore Microporous Aluminophosphates in Low-Temperature Solar Energy Storage: The Structure-Property Relationship, Adv. Funct. Mater. 22 (2012) 1952–1957. https://doi.org/10.1002/adfm.201102734.
[25] A. Krajnc, J. Varlec, M. Mazaj, A. Ristić, N.Z. Logar, G. Mali, Superior Performance of Microporous Aluminophosphate with LTA Topology in Solar-Energy Storage and Heat Reallocation, Adv. Energy Mater. 7 (2017) 1601815. https://doi.org/10.1002/aenm.201601815.
[26] Z. Liu, J. Xu, M. Xu, C. Huang, R. Wang, T. Li, X. Huai, Ultralow-temperature-driven water-based sorption refrigeration enabled by low-cost zeolite-like porous aluminophosphate, Nat. Commun. 13 (2022) 193. https://doi.org/10.1038/s41467-021-27883-4.
[27] S. Mintova, ed., Verified syntheses of zeolitic materials, 3rd revised ed, Synthesis Commission of the International Zeolite Association, S. l., 2016.
[28] A. Tuel, S. Caldarelli, A. Meden, L.B. McCusker, C. Baerlocher, A. Ristic, N. Rajic, G. Mali, V. Kaucic, NMR Characterization and Rietveld Refinement of the Structure of Rehydrated $AlPO_4$-34, J. Phys. Chem. B 104 (2000) 5697–5705. https://doi.org/10.1021/jp000455a.
[29] M.L. Carreon, S. Li, M.A. Carreon, AlPO-18 membranes for CO_2/CH_4 separation, Chem. Commun. 48 (2012) 2310. https://doi.org/10.1039/c2cc17249f.
[30] H. Reinsch, M.A. van der Veen, B. Gil, B. Marszalek, T. Verbiest, D. de Vos, N. Stock, Structures, Sorption Characteristics, and Nonlinear Optical Properties of a New Series of Highly Stable Aluminum MOFs, Chem. Mater. 25 (2013) 17–26. https://doi.org/10.1021/cm3025445.
[31] H. Furukawa, F. Gándara, Y.-B. Zhang, J. Jiang, W.L. Queen, M.R. Hudson, O.M. Yaghi, Water Adsorption in Porous Metal–Organic Frameworks and Related Materials, J. Am. Chem. Soc. 136 (2014) 4369–4381. https://doi.org/10.1021/ja500330a.
[32] M.J. Katz, Z.J. Brown, Y.J. Colón, P.W. Siu, K.A. Scheidt, R.Q. Snurr, J.T. Hupp, O.K. Farha, A facile synthesis of UiO-66, UiO-67 and their derivatives, Chem. Commun. 49 (2013) 9449–9451. https://doi.org/10.1039/C3CC46105J.
[33] G. Cao, M. Afeworki, G.J. Kennedy, K.G. Strohmaier, D.L. Dorset, Structure of an aluminophosphate EMM-8: a multi-technique approach, Acta Crystallogr. B 63 (2007) 56–62. https://doi.org/10.1107/S0108768106040109.

[34] M. Afeworki, G. Cao, D.L. Dorset, K.G. Strohmaier, G.J. Kennedy, Multinuclear and multidimensional solid-state NMR characterization of EMM-8, Microporous Mesoporous Mater. 103 (2007) 216–224. https://doi.org/10.1016/j.micromeso.2007.01.048.
[35] A. Simmen, L.B. McCusker, C. Baerlocher, The structure determination and rietveld refinement of the aluminophosphate $AlPO_4$-18, 11 (1991) 654–661. https://doi.org/10.1016/S0144-2449(05)80167-8.
[36] W. Loewenstein, The distribution of aluminum in the tetrahedra of silicates and aluminates, Am. Mineral. 39 (1954) 92–96.
[37] Z. Tahraoui, H. Nouali, C. Marichal, P. Forler, J. Klein, T.J. Daou, Influence of the Compensating Cation Nature on the Water Adsorption Properties of Zeolites, Molecules 25 (2020) 944. https://doi.org/10.3390/molecules25040944.
[38] Y. Marcus, A simple empirical model describing the thermodynamics of hydration of ions of widely varying charges, sizes, and shapes, Biophys. Chem. 51 (1994) 111–127. https://doi.org/10.1016/0301-4622(94)00051-4.
[39] G. Poulet, A. Tuel, P. Sautet, A Combined Experimental and Theoretical Evaluation of the Structure of Hydrated Microporous Aluminophosphate $AlPO_4$-18, J. Phys. Chem. B 109 (2005) 22939–22946. https://doi.org/10.1021/jp050670x.
[40] J. Varlec, A. Krajnc, M. Mazaj, A. Ristić, K. Vanatalu, A. Oss, A. Samoson, V. Kaučič, G. Mali, Dehydration of $AlPO_4$-34 studied by variable-temperature NMR, XRD and first-principles calculations, New J. Chem. 40 (2016) 4178–4186. https://doi.org/10.1039/C5NJ02838H.
[41] M. Usman, A.S. Ghanem, S. Niaz Ali Shah, M.D. Garba, M. Yusuf Khan, S. Khan, M. Humayun, A. Laeeq Khan, A Review on SAPO-34 Zeolite Materials for CO_2 Capture and Conversion, Chem. Rec. 22 (2022) e202200039. https://doi.org/10.1002/tcr.202200039.
[42] B. Mette, H. Kerskes, H. Drück, H. Müller-Steinhagen, Experimental and numerical investigations on the water vapor adsorption isotherms and kinetics of binderless zeolite 13X, Int. J. Heat Mass Transf. 71 (2014) 555–561. https://doi.org/10.1016/j.ijheatmasstransfer.2013.12.061.
[43] B.O. Nascimento, B.F. dos Santos, D.A.S. Maia, D.C. de Melo, E. Vilarrasa-Garcia, A.E.B. Torres, M. Bastos-Neto, D.C.S. Azevedo, Water adsorption in fresh and thermally aged zeolites: equilibrium and kinetics, Adsorption 27 (2021) 1043–1053. https://doi.org/10.1007/s10450-021-00331-x.
[44] M. Fischer, Water adsorption in SAPO-34: elucidating the role of local heterogeneities and defects using dispersion-corrected DFT calculations, Phys. Chem. Chem. Phys. 17 (2015) 25260–25271. https://doi.org/10.1039/C5CP04189A.
[45] K. Yang, T. Pan, I. Pinnau, Z. Shi, Y. Han, Simultaneous generation of atmospheric water and electricity using a hygroscopic aerogel with fast sorption kinetics, Nano Energy 78 (2020) 105326. https://doi.org/10.1016/j.nanoen.2020.105326.
[46] E.-P. Ng, L. Delmotte, S. Mintova, Selective Capture of Water Using Microporous Adsorbents To Increase the Lifetime of Lubricants, ChemSusChem 2 (2009) 255–260. https://doi.org/10.1002/cssc.200800234.
[47] Y. Tu, T. Zhan, T. Wu, F. Zhang, I. Kumakiri, X. Chen, H. Kita, Rapid synthesis of AlPO-18 molecular sieve for gas separation with dual-template agent, Microporous

Mesoporous Mater. 327 (2021) 111436. https://doi.org/10.1016/j.micromeso.2021.111436.